Engineering Science and Military Technologies
Volume (9) - Issue (2) - Sep 2025
ISSN: 2357- 0954
DOI:10.21608/EJMTC.2025.339987.1292

Reconfigurability techniques in microwave components : A review

Review Article

Kareem H. El-Gendy, Mohamed F. Hagag, and Mahmoud A. Abdalla

Department of Electronic Engineering, Military Technical College, Cairo, Egypt

Keywords:
Liquid metals, mechanical tuning, photoconductive switches, PIN-diodes, reconfigurable microwave components, RF MEMS, varactors.

Corresponding Author:
Kareem H. El-Gendy, Electronic Engineering Department, Military Technical College, Egypt, **Tel:** 01116900173, **E-mail:** kareemhossam@ieee.org

Received : 28 November 2024
Accepted : 05 April 2025

Abstract

Reconfigurable techniques in microwave components are essential for the flexibility and performance enhancement that current communication systems demand. This paper proposes an overview of the different techniques for reconfiguration applied in microwave components, including electrical, optical, mechanical, and material-based techniques. More attention is given to electrical reconfiguration methods, which currently dominate the applications due to their high-performance characteristics and ease of implementation. Optical reconfigurability uses photonic elements to tune microwave components. It has the advantages of high-speed modulation and immunity to electromagnetic interference. Mechanical reconfigurability uses moving parts to change the physical construction of microwave components and, consequently, allows for fine control, but usually with lower switching speeds. Material-based reconfigurability is performed by smart materials like liquid crystals and phase-change materials. It can dynamically modify the electromagnetic properties of the microwave device. This reconfigurable technique needs a complex setup and has a low switching speed. The basic principles, the advantages, and the disadvantages of each reconfigurable technique are stated. Moreover, this paper discusses the implementation of these reconfiguration techniques, including biasing and measurement setup, with their practical considerations. The main performance metrics of insertion loss, isolation, power handling capability, dynamic tuning range, and switching speed are studied..

I. INTRODUCTION

The rapid development of wireless communication technologies has greatly enhanced the demand for reconfigurable radio frequency (RF) circuits, which form a core in developing adaptable and multi-functional devices. Such circuits change their operational characteristics in real-time, providing flexibility and efficiency in several applications[1-7]. Multiple techniques are used in the tuning process of microwave components, each with advantages and limitations. Reconfigurable circuits are widely used in modern wireless applications like cognitive radio, software-defined radio, and multi-band communication systems. The reconfigurable microwave components enable a reduction in overall size and cost due to the lack of multiple dedicated circuits[8-16].

Several reconfigurability techniques have been developed in microwave components, exhibiting different advantages and limitations. The approaches can be broadly classified into electrical, optical, mechanical, and material-based reconfiguration methods, as shown in Fig. 1. For the electrical reconfiguration, it is achieved utilizing active elements such as PIN-diodes, varactors, and RF MEMS switches[17-23].

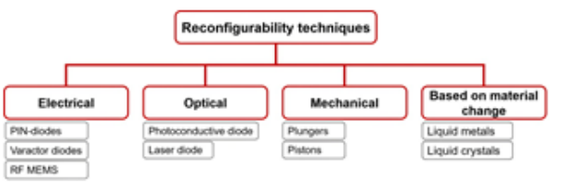

Fig. 1: Different techniques used in tuning microwave components.

In addition, optical reconfiguration methods rely on changes in RF circuit characteristics, induced by illuminating pho- photo-sensitive materials or photoconductive switches[24-28]. Moreover, the mechanical reconfiguration depends on a physical change in the geometry of the circuit. Several techniques include adjustment with structural elements or movable parts[29-35]. Furthermore, the material-based approach makes use of the unique properties of particular materials, including liquid crystals and liquid metals, to achieve reconfigurability[29-35]. While these methods have certain advantages in particular applications, the electrical reconfiguration technique remains the most adopted method

due to its high-speed switching capabilities, reliability, and simplicity in integration with conventional RF systems[36-38]. These electronic components provide precise control over circuit parameters and can be easily integrated into traditional PCB and semiconductor manufacturing processes.

The advantages and disadvantages of the different reconfigurability techniques, used in microwave components, are summarized in Table 1. Electrical switches usually possess high switching speed, compact size, and easy integration, however, they involve the requirement of a biasing network, have linearity issues, and result in higher insertion loss. On the other hand, optical switches provide high-speed operation with immunity to electromagnetic interference, without biasing wires, but come with some drawbacks like the high complexity setup, the high cost, and the lossy behavior. Moreover, mechanical switches have merits like high precision, low insertion loss, and robustness at high input power levels, but they are slower, bulkier, and require higher actuation power. Finally, material-based switches offer a wide control range, low loss for some materials, and passive operation; however, they also exhibit slower response times, temperature sensitivity, and limited applicability. Thus, each technique offers different trade-offs in terms of performance, feasibility, and application-specific needs.

First, the electrically reconfigurable microwave components are presented in Section II, including a comparison between different electrical switches. The optical and the mechanical reconfigurable techniques are then introduced in Sections III and IV, respectively. Finally, section V includes tunable microwave components based on material change.

Table 1: A comparison between different reconfigurable techniques[24,35,39,50].

Reconfigurability technique	Advantages	Disadvantages
Electrical	-Fast switching speed -Compact size -Ease of integration	-Require biasing network -Non-linearity -Lower insertion loss
Optical	-High-speed -No electromagnetic interference -No biasing wires	-High complexity -High cost -Lossy behavior
Mechanical	High precision Low insertion loss Robust at high power	-Slower -Bulkier -Higher power for actuation
Based on material change	-Broad control range -Low loss (in some materials) Passive operation	-Slow response time -Temperature sensitivity -Limited applications

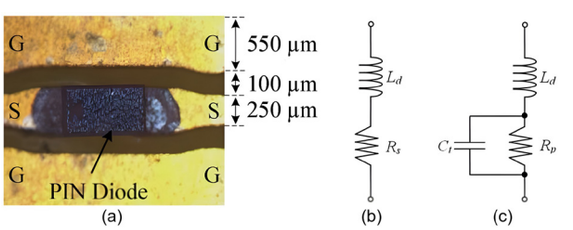

Fig. 2: (a) A PIN-diode[75] connected to a coplanar transmission line in series. The equivalent circuit of the PIN-diode (b) ON-State (Forward bias). (c) OFF-State (Reverse bias)[76].

II. ELECTRICALLY RECONFIGURABLE RF COMPONENTS

There are three major technologies used to implement electrical reconfigurability in microwave components, including PIN-diodes[17,18,51–57], varactor diodes[22,23,58-69] and RF MEMS switches[19-21,70-74]. PIN-diodes are used as a simple RF switch, varactor diodes as a variable capacitance depending on the applied voltage, and RF MEMS use mechanical movements to implement switches. They allow microwave components to be tuned electronically, enabling frequency and impedance adjustments in applications such as filters and matching networks.

A. PIN-Diodes

PIN-diodes are semiconductor devices consisting of three regions: a P-type (positive), an intrinsic (I), and an N-type (negative) region[77]. The intrinsic layer is sandwiched between the P and N regions. In this region, charge carriers recombine, allowing the diode to act as a variable resistor at high frequencies. A co-planar waveguide (CPW) transmission line with a mounted PIN-diode, connected in series, is shown in Fig. 2(a). PIN-diodes have two operational states (discrete-tuning). The equivalent circuits of the PIN-diode in its ON and OFF states are shown in Fig. 2(b) and (c), respectively. When a PIN-diode is in the ON-state, it behaves like a low

resistance to current flow, thanks to the depletion of charge carriers in the intrinsic region. Conversely, it acts as a high resistance, effectively blocking current, in its OFF state.

To use a PIN-diode in the tuning of a microwave component, a biasing network is required. It consists of a DC bias source to provide either forward or reverse bias voltage to supply the required power for turning the diode into either a high-resistance or low-resistance state. Also, an RF choke-inductor is required to keep the RF signal away from the DC bias source for handling the interaction of DC and RF signals, and allows the passage of the DC current. Moreover, a capacitor is used to decouple the RF signal from the DC bias. To set the bias current, a resistor might also be a part of the biasing network. In the parallel coupled lines bandpass filter, presented in[78], four PIN-diodes are used to control the signal level attenuation between the two ports. The top and bottom layers of the fabricated tunable filtering attenuator are shown in Fig. 3(a) and (b), respectively. As shown in Fig. 3(a), three inductors (RF chokes) connect the DC biasing source with the fabricated bandpass filter. Also, three grounded capacitors (DC blocks) are attached to the DC biasing source, as shown in Fig. 3(b). The measurement setup is shown in Fig. 3(c). The ports of the presented filtering attenuator are connected to the vector network analyzer (VNA) to measure its S-parameters, while the four PIN-diodes are connected to the DC biasing source to switch between their operational states.

The measurement results, of the fabricated filtering attenuator in[78], are shown in Fig. 4. The measured S-parameters are shown in Fig. 4(a). It can be seen that the measured transmission coefficient (S21) has an attenuation dynamic range of 14.58 dB (from –2.24 to –16.82 dB), depending on the applied biasing DC voltage (from 0 to 0.62 V). Fig. 4(a) shows that the measured attenuation level of (S21) increases with the increasing value of the biasing voltage.

Moreover, PIN-diodes are integrated with different microwave components to alter the signals' paths between their ports, as in the four-port filtering RF T-type switch in[79]. The operational states of the RF switch are shown in Fig. 5(a), each state consists of two channels. The layout of the RF switch is shown in Fig. 5(b), showing the biasing circuit of the utilized PIN-diodes. It consists of a ring resonator. Each feeding port is coupled to two half-wavelength resonators along with the ring resonator. A PIN-diode is loaded to each resonator. Switching between the ON and OFF states of the PIN-diodes, the coupling between the feeding lines and the resonators is controlled, and an operational state is identified. The simulated and the measurement results of the fabricated RF switch are shown in Fig. 6(a), (b), and (c) for states 1, 2 and 3. For state 1, the PIN-diodes (D1) are ON, while (D2 and D3) are OFF. The input signal from port 1 is coupled to port 3, while the power flow from port 2 is directed to port 4. Similarly, states 2 and 3 are identified.

For the reconfigurable wideband power divider stated in[80], two PIN-diodes are used to switch its working states between a two-way and a four-way power divider. The schematic of the power divider is shown in Fig. 7(a). The stated power

divider acts as a two-way power divider when the PIN-diodes are reverse-biased. Conversely, when the diodes are forward-biased, it acts as a two-way power divider. Photographs of the fabricated prototype are shown in Fig. 7(b) and (c) for the top and the bottom views, respectively. The biasing network consists of an AC-blocking inductor and a biasing resistor. A comparison between the simulated and the measured S-parameters of the stated power divider is shown in Fig. 8(a) and (b) for the two-way and the four-way states. An insertion loss of about 1.7 and 1.25 dB is measured for the two and four-way functions, respectively.

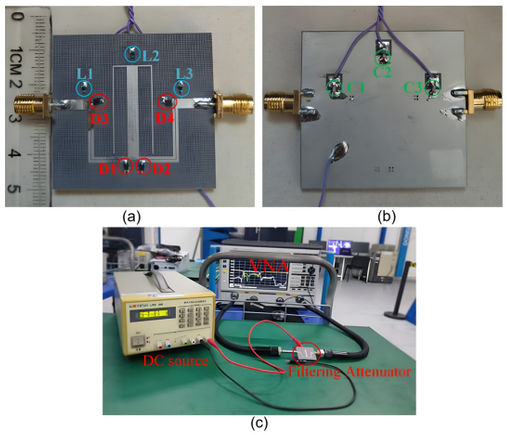

Fig. 3: The realized filtering attenuator with the measurement setup. (a) Top-view. (b) Bottom-view. (c) The measurement setup[78].

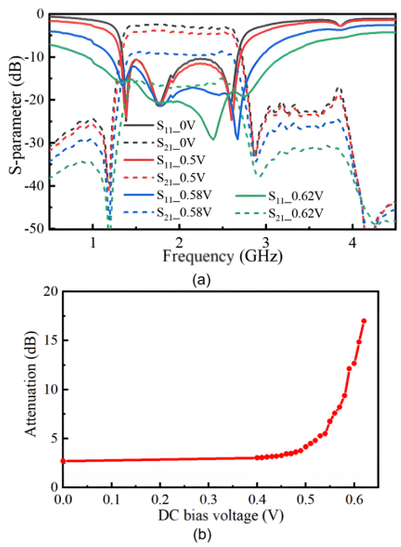

Fig. 4: The measurement results of the tunable filtering attenuator. (a) S-parameters. (b) The variation in the attenuation level with the applied DC bias voltage[78].

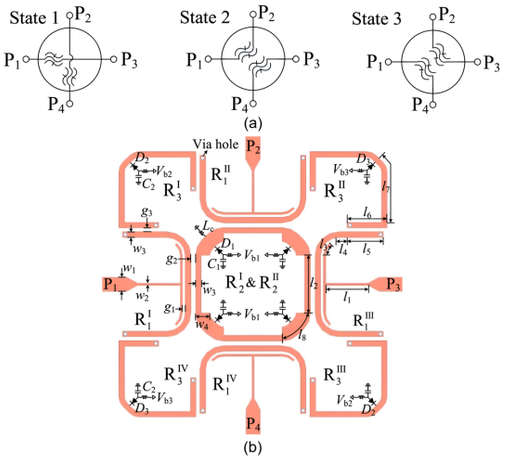

Fig. 5: (a) The schematic of the filtering RF switch, with its different operational states. (b) The Layout[79]

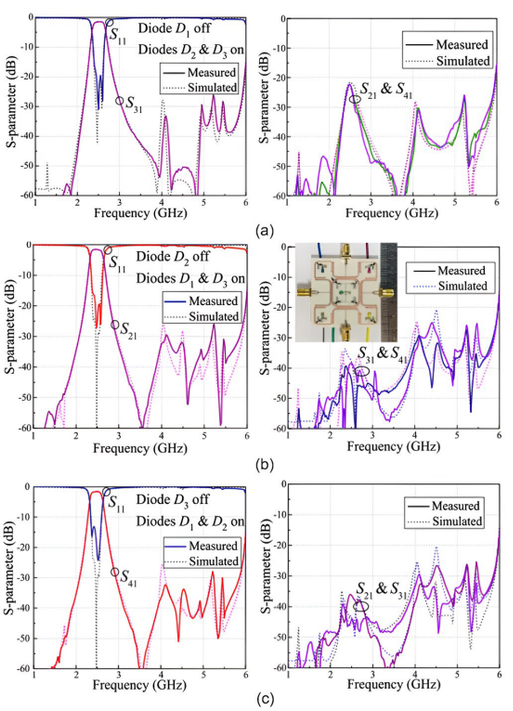

Fig. 6: The simulated and the measurement results of the filtering RF switch. (a) State 1. (b) State 2. (c) State 3[79]

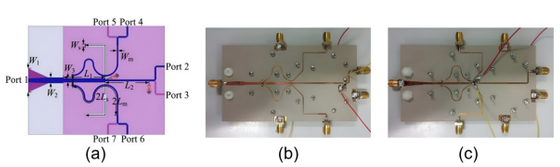

Fig. 7: Wideband reconfigurable power divider. (a) State 1 (Two-way). (b) State 2 (Four-way)[80]

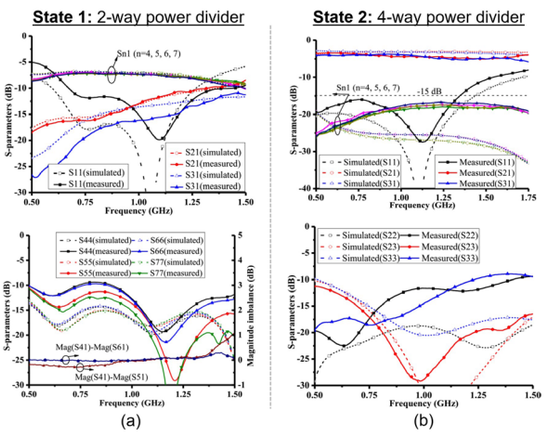

Fig. 8: The simulated and the measurement results of the wideband reconfigurable power divider. (a) State 1. (b) State 2. (c) State 3[80].

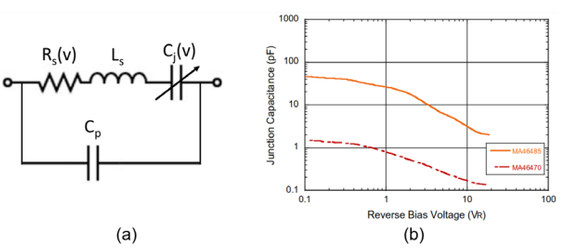

Fig. 9: For the varactor diodes, (a) The equivalent circuit. (b) An example for the variation of the junction capacitance with the supplied reverse bias voltage. (redrawn from[81])

B. VARACTOR-DIODES

Another lumped element used to electrically tune microwave components is the varactor diode (varicap). It is a semiconductor device that acts as a variable capacitor. Fig. 9(a) shows the equivalent circuit of a varactor diode. It consists of a parasitic capacitance (Cp) connected in parallel with a series resistance (Rs), a series inductance (Ls), and a series capacitance (Cj). As shown in Fig. 9(b), the capacitance (Cj) varies along with the applied reverse-bias voltage, making the varactors useful in the continuous tuning of the microwave components but with a low dynamic range[82-86].

In[87], a high-selectivity two-path mixed coupling filter was realized by adding a resonance circuit to achieve tunable transmission zeros. The two transmission zeros are controlled via the source-load coupling, as shown in Fig. 10(a). Also, two more transmission zeros are produced from the input network and tunable via the transmission line (L5). It is realized using two transmission lines electrically coupled with varactors at one end and magnetically coupled using semi-lumped through-via at the other end. It also offers flexibility in varying the coupling coefficient

in this mixed coupling approach to obtain a wide tuning range. The fabricated prototype is shown in Fig.

10(b). A biasing resistor is used with a capacitance (Cb) that acts as a DC block. A comparison between the simulated and the measured S-parameters of the fabricated tunable filter is shown in Fig. 11. As can be seen, the resonant frequency of the filter is continuously tuned with the variation of the supplied DC voltage.

Moreover, a reconfigurable dual-band coupler is presented in[88]. Its lower band is independently adjustable in resonant frequency and coupling coefficient. The fabricated prototype is shown in Fig. 12. It consists of a circular patch with four coupled line transmission lines, each connected with a varactor diode. The used diodes provide a capacitance range from 0.7 to 22.45 pF when biased with 30 to 0 Vdc. Each diode is connected with a DC block and an RF choke. A comparison between the simulated and the measured S-parameters is shown in Fig. 13(a) and (b), for the tunability in resonant frequency and coupling coefficient, respectively. The proposed work has a measured insertion loss of 2 dB.

In[89], a single-pole, double-throw (SPDT) RF switch is presented. As shown in Fig. 14(a), each two Substrate-Integrated-Waveguide (SIW) evanescent-cavity resonators are connected with each other with a pair of varactor diodes. The varactors are used to tune the transmission between resonators by adjusting the coupling among them by controlling the supplied DC bias voltage. The simulated and measured S-parameters of the RF switch are shown in Fig. 14(b) and (c), for states 1 and 2, respectively. Biasing voltages of 4.6, 7.5 and 4.6 V are supplied to the varactors connected to the resonators 1, 2, and 3, respectively.

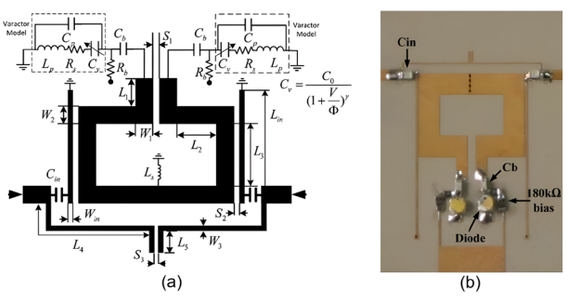

Fig. 10: (a) The configuration of the tunable filter. (b) The fabricated filter with the biasing network[87].

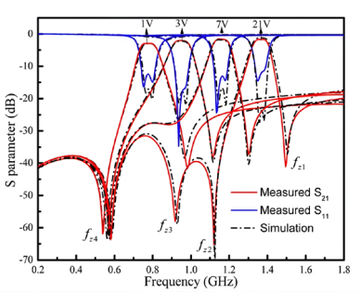

Fig. 11: A comparison between the simulated and the measured S-parameters of the tunable filter, at different biasing voltages[87]

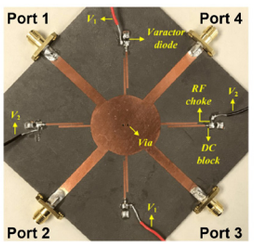

Fig. 12: The fabricated prototype of the reconfigurable dual-band coupler presented in[88].

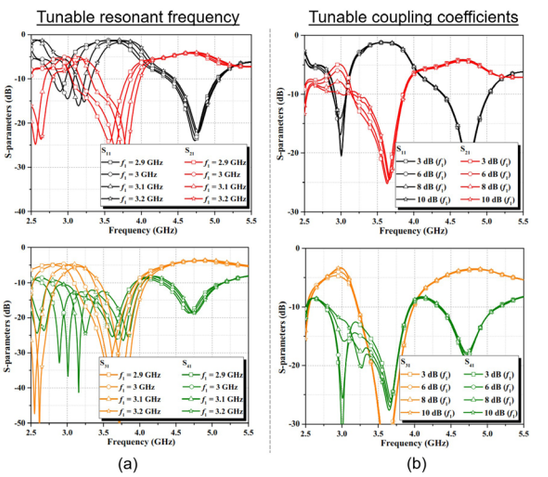

Fig. 13: For the presented dual-band coupler stated in[88]. (a) State 1 (tunable resonant frequency). (b) State 2 (tunable coupling coefficients).

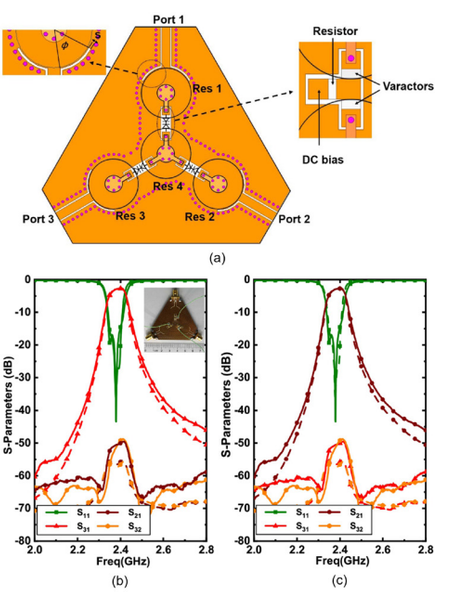

Fig. 14: (a) The geometry of the SPDT RF switch. The simulated and the measured S-parameters. (b) State 1. (c) State 2[89]

C. RF MEMS

Microwave components can also be tuned using MEMS (Micro-Electro-Mechanical Systems). They integrate mechanical and electrical components on a single chip. These systems typically range from a few micrometers to a few millimeters in size. RF MEMS have a relatively high-quality factor with a great capability to handle a wide range of frequencies[20,90]. However, they have a slow switching speed and require high control voltages. Moreover, MEMS have a limited life cycle due to the repeated mechanical movements, which lead to material degradation over time.

A frequency-tunable filter is presented in[91]. As shown in Fig. 15, it consists of two waveguide cavities, coupled with each other with an inductive iris. An RF MEMS switch is mounted to the inner wall of each cavity, as shown in Fig. 16(a), where the amplitude of the current is maximum. Changing the state of the RF MEMS switches, the distribution of the electromagnetic field of the resonant mode is perturbed, which leads to a shift in the frequency of the resonating mode as shown in Fig. 16(b). A high-quality factor of 1000 is measured. Also, a 90 V biasing voltage is used.

Table II compares different electrical switches used to tune RF components. The comparison is based on a number of key aspects, including switching speed, power handling capability, insertion loss, linearity, power consumption, reliability, and complexity. In the case of using PIN-diodes, high-speed switching response and high-power handling capability are obtained, hence they are suitable for high-power and fast switching applications. While the varactor diodes maintain a relatively lower insertion loss and low power consumption, they can handle lower power input signal levels. Furthermore, using RF MEMS provides a linear response and a very low insertion loss, but they are more sensitive to the external environment. Also, they have the slowest switching speed.

III. OPTICALLY RECONFIGURABLE RF COMPONENTS

Photoconductive switches are finding an increasingly important role in the tuning process of advanced microwave components[27,28,33,50,92-97]. They consist of semiconductor materials that change their conductivity, creating electron-hole pairs when interacting with light (laser). In this way, the state of the switch is changed with the exposure of light. Common materials for such switches are Gallium Arsenide (GaAs), Silicon (Si), and Indium Phosphide (InP), each with different performance characteristics.

Photoconductive switches offer several key advantages over traditional tuning technologies. Some of these features are the ultra-fast switching speeds in the order of picoseconds, excellent isolation during their OFF state, and a low insertion loss obtained during their ON state. Moreover, they offer high reliability, as there are no mechanical parts in their structures. Furthermore, they are biased by an optical laser source, which guarantees minimal electromagnetic interference (EMI) between the control signals (light) and the RF signals. On the other hand, using an optical laser source increases the cost and the measurement complexity, as the light source must be perfectly aligned with the used RF switches.

A SIW-SPDT switch is presented in[98]. The input signal is derived to the output ports through two SIW junctions, as shown in Fig. 17(a). A photoconductive switch is attached to the top layer of each junction. Actuating the switches, their operational states are manipulated, hence, controlling the transmission of the input RF signals through the junctions. A photograph of the fabricated prototype SIW-SPDT switch is shown in Fig. 17(b), showing the used photoconductive switches. Moreover, a comparison between the simulated and the measured S-parameters is shown in Fig. 18(a) and (b) for states 1 (PE1 OFF and PE2 ON) and 2 (PE1 ON and PE2 OFF), respectively. The results show relatively low insertion loss levels.

In[99], a waveguide SPDT switching architecture is proposed. Four embedded evanescent switch posts are used to control the transmission of RF signals as shown in Fig. 19. Each channel contains a pair of switch posts. The switches are constructed using multiple silicon wafers. The ON and OFF states of the switches are represented by simulating the posts with different conductivity values, 0.1 and 425 S/m for the ON and OFF states, respectively. The measurement setup is shown in Fig. 20(a), in which fiber optic cables are used in the photo-excitation process. The measured S-parameters of state 1, where port 2 is matched and port 3 is isolated, are shown in Fig. 20(b).

A dual-band reconfigurable bandstop filter is presented in[92]. The configuration of the proposed filter is shown in Fig. 21(a). It consists of a transmission line coupled with two split ring resonators (A and B) that differ in their resonant frequencies, which define the stop bands. A 73-um silicon chip is positioned in the gap of each resonator. A laser diode is positioned above each silicon chip, as shown in Fig. 21(b). Changing the light intensity directed to the silicon chip, its conductivity varies, and the proposed bandstop filter can switch its stopbands ON and OFF. The ON state is defined at a light intensity of 20 W/cm2 with a Si conductivity of about 2000 S/m. Furthermore, the OFF state is defined when the laser diodes are turned off. A comparison between the simulated and the measured S-parameters is shown in Fig. 21(a), (b), and (c) for states 1, 2, and 3, respectively. A measured insertion loss of 1.2 dB is obtained in the upper and lower bands. It is worth mentioning that the laser diodes should be precisely positioned above the Si chips in the measurement setup.

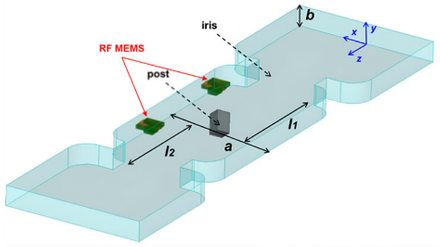

Fig. 15: The geometry of the frequency-tunable filtering waveguide. (redrawn from[91])

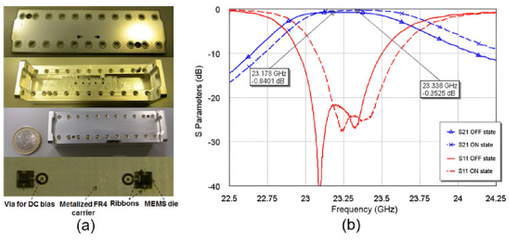

Fig. 16: For the frequency-tunable filtering waveguide, (a) The fabricated prototype. (b) The measured S-parameters[91]

Table 2: A comparison between different electrical switching mechanisms[39-49].

Mechanism	Advantages	Disadvantages
PIN-diodes	-High reliability -Low cost -Fast switching speed (ns)	-High ON-State DC bias -High power handling cap -Discrete tuning
varactor diodes	-Small current flow -Continuous tuning	-Non-linear -Low dynamic range
RF MEMS	-High isolation -High linearity -Low power loss/ noise figure	-High control voltage -Slow switching speed (µs to ms) -Limited life cycle

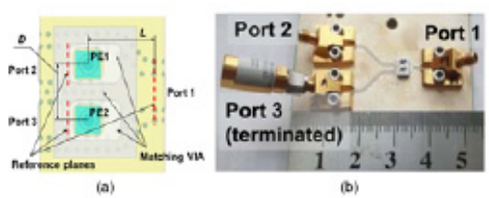

Fig. 17: For the SIW-SPDT switch, (a) The structure. (b) The fabricated prototype[98]

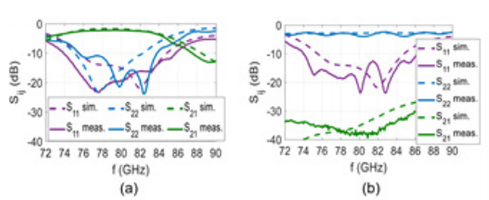

Fig. 18: A comparison between the simulated and the measured S-parameters of the SIW-SPDT switch, (a) State 1 (PE1 OFF and PE2 ON). (b) State 2 (PE1 ON and PE2 OFF)[98].

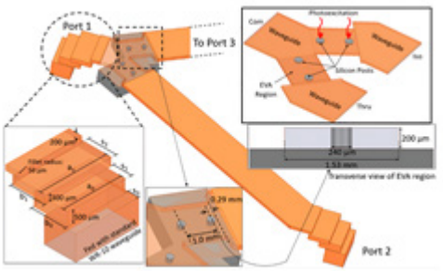

Fig. 19: The geometry of the SPDT waveguide switch, showing the embedded evanescent post switches[99].

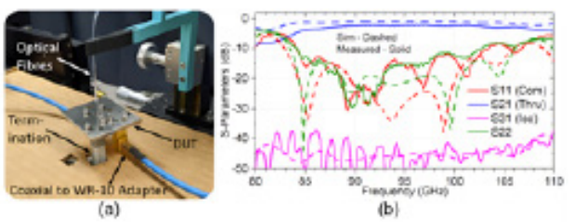

Fig. 20: For the SPDT waveguide switch. (a) The fabricated prototype with the measurement setup. (b) A comparison between the simulated and the measured S-parameters[99].

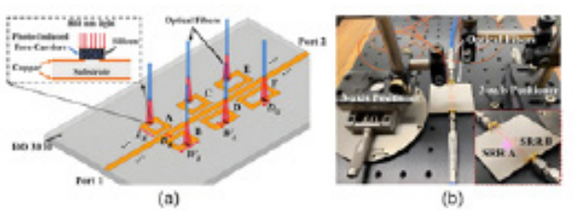

Fig. 21: For the reconfigurable bandstop filter. (a) The configuration. (b) The fabricated prototype with the biasing setup[92].

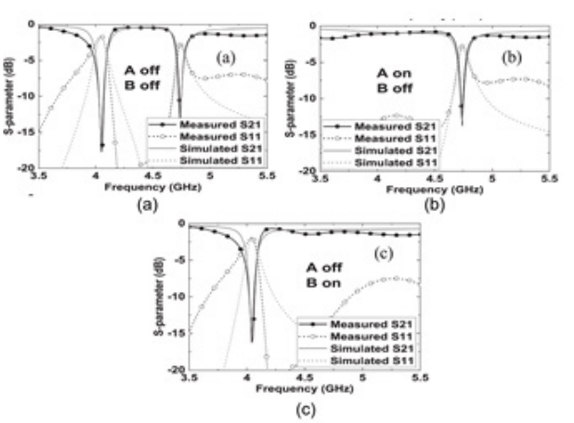

Fig. 22: A comparison between the simulated and the measured S-parameters of the reconfigurable bandstop filter. (a) State 1. (b) State 2. (c) State 3[92].

IV. MECHANICALLY RECONFIGURABLE RF COMPONENTS

Another mechanism used in tuning RF components, is the mechanical tuning technique. Simply, the performance of the RF circuit is tuned due to a certain physical adjustment in the circuit's structure. Tuning elements include plungers, rotary vane tuners, and tuning slugs[32-35, 100-104]. Using these methods provides a low insertion loss and a high-power handling capability. These advantages make the mechanical tuning competitive in applications needing reliable power handling. On the other hand, this technique has various limitations, including the relatively slow response times compared to the electrical or optical tuning techniques. Also, a higher power consumption is required for the related action mechanisms.

In[105], a fourth-order frequency-tunable filtering waveguide is introduced. As shown in Fig. 23(a), it consists of four waveguide resonators (operated in T E011 mode), in addition to a coupling one (operated in T E111 mode). The fabricated prototype of the filter is shown in the inset of Fig. 23(b). As seen, each resonator has a tuning plunger to change its length. The bandwidth of the proposed filter is tuned by changing the length of the coupling resonator. The measured S-parameters of the fabricated prototype are shown in Fig. 23(b), showing narrow and wide band responses. Moreover, the resonant frequency of the proposed filtering waveguide is tuned by modifying the lengths of all the resonators. The measured S-parameters, with different resonant frequencies, of the narrow and wide band responses are shown in Fig. 23(c) and (d), respectively.

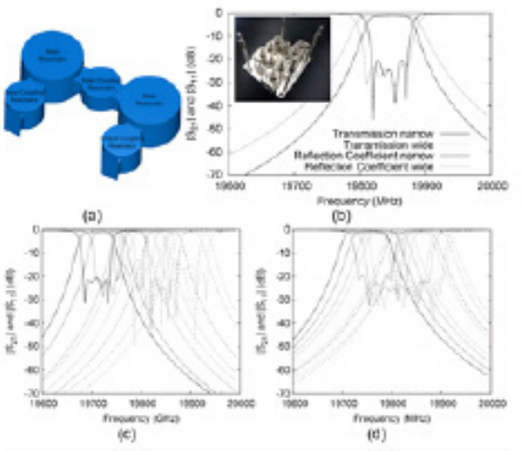

Fig. 23: For the frequency-tunable filtering waveguide, (a) A 3D geometry. (b) The measured S-parameters of the narrow / wide-band filtering responses. (c) Frequency tuning of the measured S-parameters of the narrow-band filtering response, at multiple resonant frequencies. (d) Frequency tuning of the measured S-parameters of the wide-band filtering response, at multiple resonant frequencies[105].

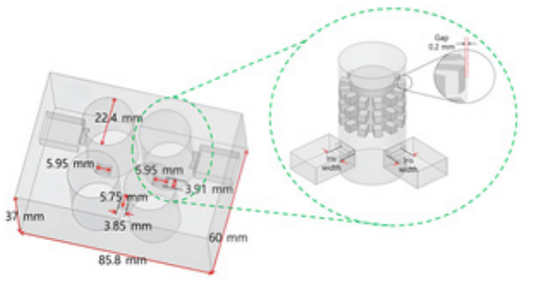

Fig. 24: The structure of the fourth-order frequency-tunable cavity filter, showing the corrugated contactless plungers[106].

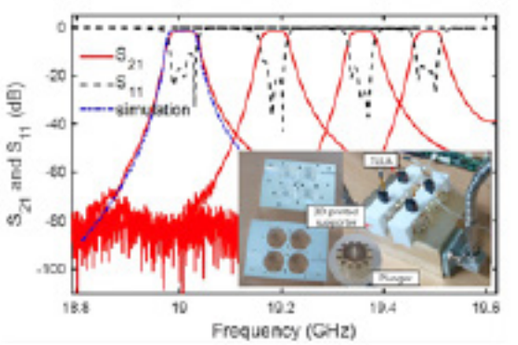

Fig. 25: A comparison between the measured and the simulated S-parameters of the frequency-tunable fourth-order cavity filter, showing the fabricated prototype and the measurement setup[106]

A corrugated contactless plunger is used in tuning the frequency of the fourth-order cavity filter presented in[106]. The structure consists of four waveguide circular resonators, connected with each other with rectangular irises, as shown in Fig. 24. The tuning process is done by moving the plunger vertically in each cavity, hence changing its resonant frequency. A 0.2 mm gap between the plunger and the resonator's side wall exists to provide contactless tuning. The fabricated prototype of the cavity filter is shown in the inset of Fig. 25, including the 3D-printed actuators and holders. A comparison between the simulated and the measured S-parameters is shown in Fig. 25, showing the variation of the resonant frequency of the proposed filter.

A reconfigurable RF power splitter is presented in[107]. The structure is based on the WR90 waveguide, as shown in Fig. 26(a). A short-circuit piston is used to mechanically tune the splitting ratio of the proposed splitter. The structure of the utilized contactless piston is shown in the inset of Fig. 26(a). The fabricated prototype is shown in Fig. 26(b). As the position of the piston varies, the division ratio of the output ports changes, as shown in Fig. 26(c).

V. RECONFIGURABLE RF COMPONENTS BASED ON MATERIAL CHANGE

Material change reconfigurability technique in RF and microwave circuits uses changing properties of materials within the circuit to affect a change in its behavior[31-35,108-113]. These involve changing the material's permittivity, permeability, or conductivity to dynamically tune circuit parameters. Liquid crystals are a class of material whose dielectric permittivity is changed by applying an external electric field, allowing for dynamic RF circuit tunability. Moreover, liquid metals have been explored recently due to their unique properties for RF circuit tuning. Commonly used liquid metals are based on gallium, indium, and tin, which are capable of remaining fluid at room temperature with high electrical and thermal conductivity.

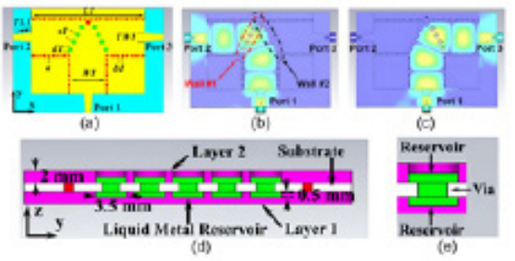

Fig. 27: For the SIW-SPDT switch, (a) The geometry. The electric field distribution. (b) State 1. (c) State 2. (d) A cross-sectional view. (e) A magnified cross-sectional view of a single via. (redrawn from[114])

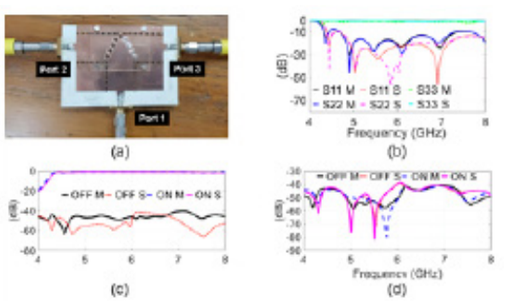

Fig. 28: For the SIW-SPDT switch, (a) The fabricated prototype. A comparison between the simulated and the measured S-parameters (b) The reflection coefficients. The transmission coefficients. (c) S21 and S31. (d) S23. (redrawn from[114]).

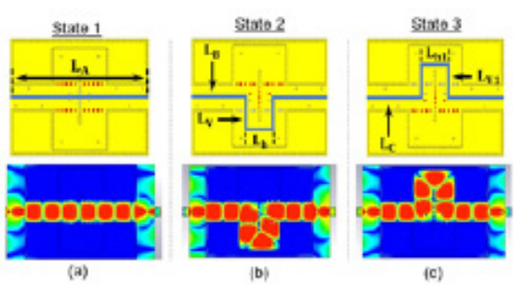

Fig. 29: For the proposed tunable phase shifter proposed in[117], the signal path with the electric field distribution of the excited mode. (a) State 1. (b) State 2. (c) State 3.

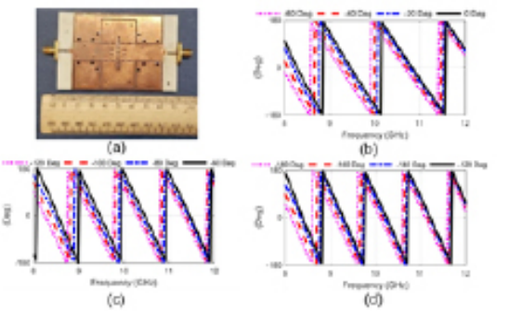

Fig. 30: For the proposed tunable phase shifter proposed in [117], (a) The fabricated prototype. A comparison between the simulated and the measured S-parameters (b) State 1. (c) State 2. (d) State 3.

In the SPDT switch presented in[114], a gallium-based liquid metal is used to control the signal's path between its output ports. The structure of the switch is shown in Fig. 27(a). The input signal is propagated through SIW transmission lines. The switch has two operational states, state 1 (a channel is created between ports 1 and 2) and state 2 (a channel is created between ports 1 and 3). A removable wall, composed of a series of drill holes, is positioned in the SIW transmission line connected to each output port, as shown in Fig. 27(a). When a channel needs to be disabled, the propagation to its output port is blocked, and the vias-wall is needed. So, the holes are filled with a gallium-based liquid metal, creating vias. When the wall is no longer required, the liquid metal is removed from the holes. The electric field distributions are shown in Fig. 27(b) and (c) for states 1 and 2, respectively. Two reservoir layers are implemented as shown in Fig. 27(d) and (e). The holes are being emptied and filled using a syringe. Removing residues after filling out the liquid metal from the vias must be considered.

The fabricated prototype of the proposed SIW-SPDT switch is shown in Fig. 28(a). The vias-wall connected to port 3 is filled with liquid metal, while the one connected to port 2 is empty (state 1). A comparison between the simulated and the measured S-parameters (state 1) is shown in Fig. 28(b), (c), and (d). As can be seen in Fig 28(a), port 1 and port 2 are matched while port 3 is unmatched. A low measured insertion loss and high isolation levels are shown in Fig. 27(c) and (d).

Additionally, a tunable SIW phase shifter is presented in[115]. The input power flow is switched between three different paths. Each path has a different electrical length. A number of vias act as barriers against the direction of the power flow, enabling the switching mechanism. Fig. 29(a), (b), and (c) show the operating states of the proposed phase shifter for states 1, 2, and 3, respectively. For example, the first state has a phase shift of -60° and is defined when the upper and the lower vias are filled with liquid metal. Moreover, states 2 and 3 provide a -120° and -180° phase shift, respectively. Fig. 30 shows a photograph of the fabricated prototype. The measured phase shift is shown in Fig. 30(b), (c), and

(d) for the states 1, 2, and 3, respectively.

Twelve fluidic channels are used to tune the resonant frequency of the branch-line coupler proposed in[115]. The channels are distributed in each branch, as shown in Fig. 31(a). The proposed coupler has two reconfigurable states; state 1 is defined when all the channels are empty, while state 2 is defined when the channels' slots are filled with ethyl acetate. A photograph of the fabricated prototype is shown in Fig. 31(b), showing the channels' slots. A syringe is used to fill the channels with the utilized liquid. A comparison between the measured and simulated S-parameters is shown in Fig. 32(a) and (b), for cases 1 and 2, respectively. The proposed coupler has a tuning range of 410 MHz.

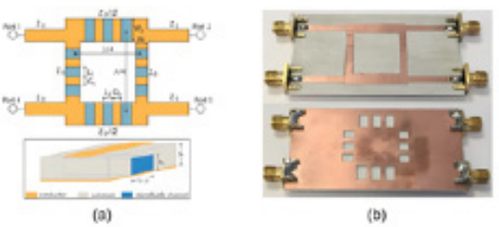

Fig. 31: For the proposed frequency-tunable branch-line coupler. (a) The configuration. (b) The fabricated prototype[115].

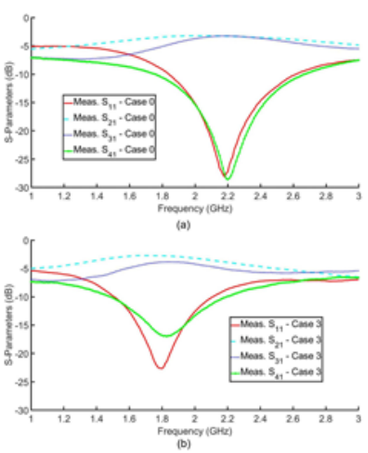

Fig. 32: A comparison between the simulated and the measured S-parameters of the proposed frequency-tunable branch-line coupler. (a) State 1 (channels are empty). (b) State 2 (channels are filled)[115].

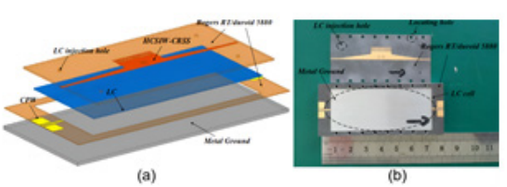

Fig. 33: For the frequency-tunable planar cavity filter, (a) A 3D geometry, showing the liquid crystal tank. (b) The fabricated prototype[116].

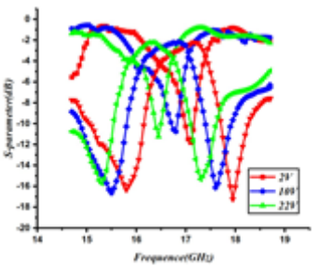

Fig. 34.: The measured S-parameters of the frequency-tunable planar cavity filter at different biasing voltages[116].

Moreover, liquid crystal is used in tuning the resonant frequency of the planar waveguide filter presented in[116]. The structure of the filter is shown in Fig. 33(a). It consists of two vertically aligned substrates on top of a metalized layer. The lower substrate acts as a liquid crystal tank, while the upper substrate contains a half-mode corrugated SIW array of quarter-wave open-circuit stubs, with a single complementary split ring resonator (CSRR) cell. The modulation voltage is applied to the liquid crystal layer. Input feeding ports consist of a co-planar waveguide structure. The liquid crystal is filled through a drilled hole in the upper substrate. A photograph of the fabricated filter is shown in Fig. 33(b). A 1 kHz square wave modulation voltage (ranging from 0V to 30V) is applied through a function generator. Varying the applied voltage, the orientation of the liquid crystal molecules is changed, and the resonant frequency of the proposed filter is tuned, as shown in Fig. 34.

VI. CONCLUSION

A comprehensive review of reconfigurable microwave components and various techniques of implementation is introduced. The analysis of various methods of reconfiguration suggests that electrical reconfiguration remains the primary method of reconfiguration, owing to its reliability, fast switching time, and compatibility with existing RF systems. While PIN-diodes, varactors, and RF MEMS switches remain the mainstream solutions, alternative techniques such as optical, mechanical, and material-based reconfiguration offer unique advantages in specific applications, despite their limited widespread adoption. In summary, as wireless communication systems continue to advance, the importance of reconfigurable microwave components in meeting the demands of future applications will escalate proportionally.

REFERENCES

[1] G. L. Matthaei, "Narrow-band, fixed-tuned, and tunable bandpass filters with zig-zag hairpin-comb resonators," IEEE Transactions on Microwave Theory and Techniques, vol. 51, no. 4, pp. 1214–1219, 2003.
[2] N. Manh-Tai, W. D. Yan, and E. P. W. Horne, "Broadband tunable filters using high Q passive tunable ICs," in IEEE MTT-S International Microwave Symposium Digest. IEEE, 2008, pp. 951–954.
[3] Y. C. Li and Q. Xue, "Tunable balanced bandpass filter with constant bandwidth and high common-mode suppression," IEEE Transactions on Microwave Theory and Techniques, vol. 59, no. 10, pp. 2452–2460, 2011.
[4] W. L. Jones, "Design of tunable combline filters of near-constant

bandwidth," Electronics Letters, vol. 1, no. 6, pp. 156–158, 1965.
[5] J.-S. Hong, "Reconfigurable planar filters," IEEE Microwave Magazine, vol. 10, no. 6, pp. 73–83, 2009.
[6] M. A. El-Tanani and G. M. Rebeiz, "Corrugated microstrip coupled lines for constant absolute bandwidth tunable filters," IEEE Transactions on Microwave Theory and Techniques, vol. 58, no. 4, pp. 956–963, 2010.
[7] M. Armendariz, V. Sekar, and K. Entesari, "Tunable SiW bandpass filters with PIN diodes," in European Microwave Conference. IEEE, 2010, pp. 830–833.
[8] W. D. Yan and R. R. Mansour, "Tunable dielectric resonator bandpass filter with embedded MEMS tuning elements," IEEE Transactions on Microwave Theory and Techniques, vol. 55, no. 1, pp. 154–160, 2007.
[9] R. V. Snyder, "A wide-band tunable filter technique based on double-diplexing and low-q tuning elements," in IEEE MTT-S International Microwave Symposium Digest. IEEE, 2000, pp. 1759–1762.
[10] S.-J. Park, I. Reines, C. Patel, and G. M. Rebeiz, "High-q rf-mems 4–6-GHz tunable evanescent-mode cavity filter," IEEE Transactions on Microwave Theory and Techniques, vol. 58, no. 2, pp. 381–389, 2010.
[11] F. Sammoura and L. Lin, "Micromachined w-band polymeric tunable iris filter," Microsystem Technologies, vol. 17, no. 3, pp. 411–416, 2011.
[12] D. Psychogiou and D. Peroulis, "Tunable VHF miniaturized helical filters," IEEE Transactions on Microwave Theory and Techniques, vol. 62, no. 2, pp. 282–289, 2014.
[13] D. Psychogiou, D. Peroulis, Y. Li, and C. Hafner, "V-band bandpass filter with continuously variable centre frequency," IET Microwaves, Antennas and Propagation, vol. 7, no. 8, pp. 701–707, 2013.
[14] E. J. Naglich, D. Peroulis, and W. J. Chappell, "Wide spurious free range positive-to-negative inter-resonator coupling structure for reconfigurable filters," in IEEE MTT-S International Microwave Symposium Digest. IEEE, 2013, pp. 1–4.
[15] R. R. Mansour, "High-q tunable dielectric resonator filters," IEEE Microwave Magazine, vol. 10, no. 6, pp. 84–98, 2009.
[16] X. Liu, L. P. B. Katehi, W. J. Chappell, and D. Peroulis, "High-q tunable microwave cavity resonators and filters using soi-based rf mems tuners," Journal of Microelectromechanical Systems, vol. 19, no. 4, pp. 774–784, 2010.
[17] A. Bandyopadhyay, P. Sarkar, T. Mondal, and R. Ghatak, "A high selective tri-band bandpass filter with switchable passband states," International Journal of Microwave and Wireless Technologies, vol. 12, no. 2, pp. 103–108, 2020.
[18] S. Kingsly, M. Kanagasabai, G. N. A. Mohammed, S. Subbaraj, Y. P. Selvam, and R. Natarajan, "Multi-band reconfigurable microwave filter using dual concentric resonators," International Journal of RF and Microwave Computer-Aided Engineering, vol. 28, no. 6, p. e21290, 2018.
[19] A.-Q. Liu, RF MEMS Switches and Integrated Switching Circuits. Springer Science and Business Media, 2010, vol. 5.
[20] G. M. Rebeiz, RF MEMS: theory, design, and technology. John Wiley and Sons, 2004.
[21] L. Pelliccia, F. Cacciamani, P. Farinelli, and R. Sorrentino, "High- q tunable waveguide filters using ohmic RF MEMS switches," IEEE Transactions on Microwave Theory and Techniques, vol. 63, no. 10, pp. 3381–3390, 2015.
[22] L. Gao and G. M. Rebeiz, "A 0.97–1.53-GHz tunable four-pole bandpass filter with four transmission zeroes," IEEE Microwave and Wireless Components Letters, vol. 29, no. 3, pp. 195–197, 2019.
[23] A. Ebrahimi, T. Baum, J. Scott, and K. Ghorbani, "Continuously tunable dual-mode bandstop filter," IEEE Microwave and Wireless Components Letters, vol. 28, no. 5, pp. 419–421, 2018.
[24] A. Fisher, Z. V. Missen, T. R. Jones, and D. Peroulis, "A fiber-free DC-7 GHz 35 W integrated semiconductor plasma switch," in IEEE MTT-S International Microwave Symposium Digest, Atlanta, GA, USA, 2021, pp. 27–30.
[25] T. R. Jones, A. Fisher, D. W. Barlage, and D. Peroulis, "A W-band photoconductive evanescent-mode waveguide switch," in IEEE MTT-S International Microwave Symposium Digest, Denver, CO, USA, 2022, pp. 959–962.
[26] Y. Chen, L. Zhang, Y. He, W. Li, and S.-W. Wong, "A pattern reconfigurable SIW horn antenna realized by PIN diode switches," in Proceedings of Computing, Communications and IoT Applications (ComComAp), Shenzhen, China, 2021, pp. 112–115.
[27] Y. Gao, M. Khaliel, F. Zheng, and T. Kaiser, "Rotman lens based hybrid analog-digital beamforming in massive MIMO systems: Array architectures, beam selection algorithms and experiments," IEEE Transactions on Vehicular Technology, vol. 66, no. 10, pp. 9134–9148, 2017.
[28] E. T. Der, T. R. Jones, and M. Daneshmand, "Miniaturized 4 × 4 Butler matrix and tunable phase shifter using ridged half-mode substrate integrated waveguide," IEEE Transactions on Microwave Theory and Techniques, vol. 68, no. 8, pp. 3379–3388, 2020.
[29] G. F. Craven and C. K. Mok, "The design of evanescent mode waveguide bandpass filters for a prescribed insertion loss characteristic," IEEE Transactions on Microwave Theory and Techniques, vol. 19, no. 3, pp. 295–308, 1971.
[30] R. J. Cameron, C. M. Kudsia, and R. R. Mansour, Microwave Filters for Communication Systems. Hoboken, NJ, USA: Wiley, March 2018.
[31] S. Sze and K. K. Ng, Physics of Semiconductor Devices. Hoboken, NJ, USA: Wiley, 2006.
[32] H. Chen, W. Che, T. Zhang, Y. Chao, and W. Feng, "SIW SPDT switch based on switchable HMSIW units," in Proceedings of IEEE International Workshop on Electromagnetics, Applications and Student Innovation Competition (iWEM), Nanjing, China, 2016, pp. 1–3.
[33] E. Shepeleva, M. Makurin, G. Evtyushkin, A. Lukyanov, A. Vilenskiy, S. Chernyshev, and M. Ivashina, "Integrated w-band photoconductive switches in siw technology," IEEE Microwave and Wireless Components Letters, vol. 31, no. 7, pp. 865–868, 2021.
[34] I. Lim and S. Lim, "Substrate-integrated-waveguide (SIW) single- pole-double-throw (SPDT) switch for X-band applications," IEEE Microwave and Wireless Components Letters, vol. 24, no. 8, pp. 536–538, 2014.
[35] X. Zhao, O. Glubokov, and J. Oberhammer, "A silicon-micromachined waveguide platform with axial ports for integrated sub-THz filters," IEEE Transactions on Microwave Theory and Techniques, vol. 70, no. 2, pp. 1221–1232, 2022.
[36] A. I. Abunjaileh and I. C. Hunter, "Tunable bandpass and bandstop filters based on dual-band combline structures," IEEE Transactions on Microwave Theory and Techniques, vol. 58, no. 12, pp. 3710–3719, 2010.
[37] R. Go´mez-Garc´ıa, J.-M. Mun˜oz-Ferreras, and D. Psychogiou, "Fully-reconfigurable bandpass filter with static couplings and intrinsic-switching capabilities," in IEEE MTT-S International Microwave Symposium Digest. IEEE, 2017, pp. 1–3.
[38] B. Yassini, M. Yu, and B. Keats, "A ka-band fully tunable cavity filter," IEEE Transactions on Microwave Theory and Techniques, vol. 60, no. 12, pp. 4002–4012, 2012.
[39] W. Feng, Y. Shang, W. Che, R. Gomez-Garcia, and Q. Xue, "Multifunctional reconfigurable filter using transversal signal-interaction concepts," IEEE Microwave and Wireless Components Letters, vol. 27, no. 11, pp. 980–982, 2017.
[40] H. Nachouane, A. Najid, A. Tribak, and F. Riouch, "A switchable bandstop-to-bandpass reconfigurable filter for cognitive radio applications," International Journal of Microwave and Wireless Technologies, vol. 9, no. 4, pp. 765–772, 2017.
[41] J. Xu, "A microstrip switchable filter with four operating modes," IEEE Microwave and Wireless Components Letters, vol. 26, no. 2, pp. 101–103, 2016.
[42] H. A. Mohamed, H. B. El-Shaarawy, E. A. F. Abdallah, and H. M. El-Hennawy, "Frequency-reconfigurable microstrip filter with dual-mode resonators using RF pin diodes and DGS," International Journal of Microwave and Wireless Technologies, vol. 7, no. 6, pp. 661–669, 2015.
[43] K. Rabbi and D. Budimir, "Highly selective reconfigurable filter for UWB systems," IEEE Microwave and Wireless Components Letters, vol. 24, no. 3, pp. 146–148, 2014.
[44] P.-H. Deng, J.-T. Tsai, and R.-C. Liu, "Design of a switchable microstrip dual-band lowpass-bandpass filter," IEEE Microwave and Wireless Components Letters, vol. 24, no. 9, pp. 599–601, 2014.
[45] E. E. Djoumessi, M. Chaker, and K. Wu, "Varactor-tuned quarter-wavelength dual-bandpass filter," IET Microwaves, Antennas and Propagation, vol. 3, no. 1, pp. 117–124, 2009.
[46] X. Huang, Q. Feng, and Q. Xiang, "Bandpass filter with tunable bandwidth using quadruple-mode stub-loaded resonator," IEEE Microwave and Wireless Components Letters, vol. 22, no. 4, pp. 176–178, 2012.
[47] B. Pal, M. K. Mandal, and S. Dwari, "Varactor tuned dual-band band-pass filter with independently tunable band positions," IEEE Microwave and Wireless Components Letters, vol. 29, no. 4, pp. 255–257, 2019.
[48] J. Guo, B. You, and G. Q. Luo, "A miniaturized eighth-mode substrate-integrated waveguide filter with both tunable center frequency and bandwidth," IEEE Microwave and Wireless Components Letters, vol. 29, no. 7, pp. 450–452, 2019.
[49] D. Tian, Q. Feng, and Q. Xiang, "A fully tunable two-pole bandpass filter using the resonator with asymmetrical capacitances," Microwave and Optical Technology Letters, vol. 61, no. 12, pp. 2843–2846, 2019.
[50] E. T. Der, T. R. Jones, and M. Daneshmand, "A miniaturized 28 GHz

4 × 4 Butler matrix using shielded ridged half-mode SIW," in IEEE MTT-S International Microwave Symposium Digest, Atlanta, GA, USA, 2021, pp. 776–779.
[51] A. Bandyopadhyay, P. Sarkar, T. Mondal, and R. Ghatak, "A dual function reconfigurable bandpass filter for wideband and tri-band operations," IEEE Transactions on Circuits and Systems II: Express Briefs, vol. 68, no. 6, pp. 1892–1896, 2020.
[52] F. Qiu, J. Huang, D. Lei, Z. Tang, and M. Yao, "Dual-band to triband to quad-band passband switchable bandpass filter," Microwave and Optical Technology Letters, vol. 59, no. 9, pp. 2307–2311, 2017.
[53] N. Kumar and Y. K. Singh, "Compact tri to dual passband switchable bandpass filter using stub-loaded split-ring resonator with improved bandwidth," Electronics Letters, vol. 51, no. 19, pp. 1510–1512, 2015.
[54] J. Mazloum, A. Jalali, and M. Ojaroudi, "Miniaturized reconfigurable band-pass filter with electronically controllable for wimax/wlan applications," Microwave and Optical Technology Letters, vol. 56, no. 2, pp. 509–512, 2014.
[55] P.-H. Deng and J.-H. Jheng, "A switched reconfigurable high-isolation dual-band bandpass filter," IEEE Microwave and Wireless Components Letters, vol. 21, no. 2, pp. 71–73, 2011.
[56] X.-J. Liao, H.-C. Yang, and N. Han, "A switchable bandpass filter using pin diodes on/off characteristics for WLAN application," Journal of Electromagnetic Waves and Applications, vol. 25, no. 10, pp. 1402–1411, 2011.
[57] J. Xu, F. Liu, and Z.-Y. Feng, "Single-/dual-band bandpass filter-integrated single-pole double-throw switch using distributed coupling tri-mode resonators," IEEE Transactions on Microwave Theory and Techniques, vol. 68, no. 2, pp. 741–749, 2019.
[58] N. Kumar, S. Narayana, and Y. K. Singh, "Constant absolute bandwidth tunable symmetric and asymmetric bandpass responses based on reconfigurable transmission zeros and bandwidth," IEEE Transactions on Circuits and Systems II: Express Briefs, vol. 69, no. 3, pp. 1014–1018, 2021.
[59] D. Tang, H. J. Qian, Y. Dong, and X. Luo, "Compact 1.75–2.7 ghz tunable bpf with wide stopband up to 9.5 ghz using harmonic-controlled sidgs resonators," IEEE Transactions on Circuits and Systems II: Express Briefs, vol. 69, no. 11, pp. 4228–4232, 2022.
[60] B. Pal, M. K. Mandal, M. Kahar, and S. Dwari, "Filtering attenuator with electronically tunable attenuation," in 2021 IEEE MTT-S International Microwave and RF Conference (IMARC). IEEE, 2021, pp.1–4.
[61] W.-L. Zhan, J.-X. Xu, and X. Y. Zhang, "Filtering t-type switch with flexible signal routing reconfigurability for crossover-/adjacent-channel applications," IEEE Microwave and Wireless Components Letters, vol. 32, no. 7, pp. 863–866, 2022.
[62] Y.-J. Zhang, J. Cai, and J.-X. Chen, "Wideband varactor-tuned balanced bandpass filter with stable passband selectivity," International Journal of RF and Microwave Computer-Aided Engineering, vol. 28, no. 9, p. e21429, 2018.
[63] T. Zhang, Z. Cai, Y. Yang, J. Bao, and Y. Wang, "Compact tunable lowpass filter with sharp roll-off and low insertion loss," Microwave and Optical Technology Letters, vol. 59, no. 10, pp. 2619–2623, 2017.
[64] W. Qin, J. Cai, Y.-L. Li, and J.-X. Chen, "Wideband tunable bandpass filter using optimized varactor-loaded SIRs," IEEE Microwave and Wireless Components Letters, vol. 27, no. 9, pp. 812–814, 2017.
[65] Z.-H. Chen and Q.-X. Chu, "Dual-band reconfigurable bandpass filter with independently controlled passbands and constant absolute bandwidths," IEEE Microwave and Wireless Components Letters, vol. 26, no. 2, pp. 92–94, 2016.
[66] M. Fan, K. Song, L. Yang, and R. Go´mez-Garcia, "Frequency-reconfigurable input-reflectionless bandpass filter and filtering power divider with constant absolute bandwidth," IEEE Transactions on Circuits and Systems II: Express Briefs, vol. 68, no. 7, pp. 2424–2428, 2021.
[67] M. Fan, K. Song, L. Yang, and R. Go´mez-Garc´ıa, "Frequency-tunable constant-absolute-bandwidth single-/dual-passband filters and diplexers with all-port-reflectionless behavior," IEEE Transactions on Microwave Theory and Techniques, vol. 69, no. 2, pp. 1365–1377, 2021.
[68] Z. Cao, X. Bi, and Q. Xu, "Tunable reflectionless filter with independently controllable dual passbands and absorbed harmonic signals," IEEE Transactions on Circuits and Systems II: Express Briefs, vol. 68, no. 11, pp. 3416–3420, 2021.
[69] S.-W. Jeong, T.-H. Lee, and J. Lee, "Frequency- and bandwidth-tunable absorptive bandpass filter," IEEE Transactions on Microwave Theory and Techniques, vol. 67, no. 6, pp. 2172–2180, 2019.
[70] Y.-C. Lee, L.-K. Wang, Y.-C. Chuang, H.-C. Hong, and Y. Chiu, "Electrothermal tunable MEMS oscillators for mems-based reservoir computing," IEEE Sensors Letters, vol. 8, no. 7, pp. 1–4, 2024.
[71] R. Alcorta Galva´n, C. Croe¨nne, B. Dubus, B. Loiseaux, E. Eustache, M. Bertrand, and A.-C. Hladky-Hennion, "Switchable saw resonators and ladder filters composed of interdigitated combs," IEEE Transactions on Ultrasonics, Ferroelectrics, and Frequency Control, vol. 71, no. 10, pp. 1302–1313, 2024.
[72] L. Han, Y. Wang, Q. Wu, S. Zhang, S. Wang, and M. Li, "A novel low- loss four-bit bandpass filter using rf mems switches," Chinese Physics B, vol. 31, no. 1, p. 018506, 2022.
[73] N. Habbachi and K. Besbes, "RF MEMS filter based on dual liquid variations," Journal of Micromechanics and Microengineering, vol. 32, no. 6, p. 065002, 2022.
[74] F. Giacomozzi, E. Proietti, G. Capoccia, G. M. Sardi, G. Bartolucci, J. Iannacci, G. Tagliapietra, B. Margesin, and R. Marcelli, "Design of u-shaped frequency tunable microwave filters in mems technology," Sensors, vol. 23, no. 1, p. 466, 2023.
[75] "Ma-com technology solutions, ma4agp907 and ma4agfcp910 algaas flip chip pin diodes."
[76] A. Clemente, L. Dussopt, R. Sauleau, P. Potier, and P. Pouliguen, "1-bit reconfigurable unit cell based on pin diodes for transmit-array applications in x-band," IEEE Transactions on Antennas and Propagation, vol. 60, no. 5, pp. 2260–2269, 2012.
[77] P. Bacon, D. Fischer, and R. Lourens, "Overview of RF SwitchTechnology and Applications." Microwave Journal, vol. 57, no. 7, 2014.
[78] W. He, J. Li, K.-D. Xu, S. Yan, and J. Chen, "Voltage-controlled tunable filtering attenuator using pin diodes," IEEE Transactions on Circuits and Systems II: Express Briefs, vol. 71, no. 2, pp. 562–566, 2024.
[79] W.-L. Zhan, J.-X. Xu, and X. Y. Zhang, "Filtering t-type switch with flexible signal routing reconfigurability for crossover-/adjacent-channel applications," IEEE Microwave and Wireless Components Letters, vol. 32, no. 7, pp. 863–866, 2022.
[80] K. Song, X. Zou, Y. Zhou, and Y. Fan, "Miniaturized ultrawideband reconfigurable power divider based on slotline and double-sided parallel-strip line," IEEE Transactions on Microwave Theory and Techniques, vol. 69, no. 4, pp. 2130–2137, 2021.
[81] "Ma-com technology solutions, ma464xx series gaas hyperabrupt var- actor diodes."
[82] W.-J. Zhou and J.-X. Chen, "High-selectivity tunable balanced bandpass filter with constant absolute bandwidth," IEEE Transactions on Circuits and Systems II: Express Briefs, vol. 64, no. 8, pp. 917–921, 2017.
[83] P.-L. Chi and T. Yang, "Novel 1.5-1.9 GHz tunable single-to-balanced bandpass filter with constant bandwidth," IEEE Microwave and Wireless Components Letters, vol. 26, no. 12, pp. 972–974, 2016.
[84] Z.-H. Chen and Q.-X. Chu, "Reconfigurable bandpass filter with electric coupling and constant absolute bandwidth," Microwave and Optical Technology Letters, vol. 58, no. 6, pp. 1401–1404, 2016.
[85] N. Kumar and Y. K. Singh, "Compact constant bandwidth tunable wideband BPF with second harmonic suppression," IEEE Microwave and Wireless Components Letters, vol. 26, no. 11, pp. 870–872, 2016.
[86] C.-W. Tang and W.-C. Chen, "A compact tunable notch filter with wide constant absolute bandwidth," IEEE Microwave and Wireless Components Letters, vol. 25, no. 3, pp. 151–153, 2015.
[87] C. Ge and X.-W. Zhu, "Highly-selective tunable bandpass filter with two-path mixed coupling," IEEE Microwave and Wireless Components Letters, vol. 24, no. 7, pp. 451–453, 2014.
[88] Y. F. Pan, S. Y. Zheng, W. Hong, and W. S. Chan, "Highly re-configurable dual-band coupler with independently tunable frequency and coupling coefficient at the lower band," IEEE Transactions on Industrial Electronics, vol. 68, no. 3, pp. 2408–2416, 2020.
[89] J. Lai, T. Yang, P.-L. Chi, and R. Xu, "1.866–2.782-ghz reconfigurable filtering single-pole-multithrow switches based on evanescent-mode cavity resonators," IEEE Transactions on Microwave Theory and Techniques, vol. 69, no. 2, pp. 1355–1364, 2021.
[90] K. Y. Chan, R. Ramer, and R. R. Mansour, "ku-band channel aggregation waveguide filters by rf mems-based detuning," IEEE Transactions on Microwave Theory and Techniques, vol. 68, no. 2, pp. 750–761, 2019.
[91] L. Pelliccia, F. Cacciamani, P. Farinelli, and R. Sorrentino, "High-q tunable waveguide filters using ohmic RF MEMS switches," IEEE Transactions on Microwave Theory and Techniques, vol. 63, no. 10, pp. 3381–3390, 2015.
[92] P. Li, Y. Shi, Y. Deng, P. Fay, and L. Liu, "Tunable and reconfigurable bandstop filters enabled by optically controlled switching elements,"

Electronics Letters, vol. 58, no. 25, pp. 985–987, 2022.
[93] E. Shepeleva, M. Makurin, A. Lukyanov, A. R. Vilenskiy, S. L. Chernyshev, and M. V. Ivashina, "Low-loss k-band photoconductive switches in siw technology," in 2020 50th European Microwave Conference (EuMC). IEEE, 2021, pp. 538–541.
[94] E. T. Der, T. R. Jones, A. Fisher, K. Moez, D. W. Barlage, and D. Peroulis, "Design and characterization of w-band silicon micromachined high-power and high-speed photoconductive evanescent-mode waveguide single and double throw switches," IEEE Transactions on Microwave Theory and Techniques, 2023.
[95] M. Haghighat, T. Darcie, and L. Smith, "Demonstration of a terahertz coplanar-strip spoof-surface-plasmon-polariton low-pass filter," Scientific Reports, vol. 14, no. 1, p. 182, 2024.
[96] P. Li, E. Zahedi, Y. Shi, Y. Deng, and L. Liu, "Dynamically tuning and reconfiguring microwave bandpass filters using optical control of switching elements," Microwave and Optical Technology Letters, vol. 66, no. 2, p. e34082, 2024.
[97] T. R. Jones, A. Fisher, D. W. Barlage, and D. Peroulis, "A w-band photoconductive evanescent-mode waveguide switch," in 2022 IEEE/MTT-S International Microwave Symposium-IMS 2022. IEEE, 2022, pp. 959–962.
[98] E. T. Der, T. R. Jones, A. Fisher, M. D. Sinanis, K. Moez, D. W. Barlage, and D. Peroulis, "A w-band spdt photoconductive evanescent-mode waveguide switch," IEEE Microwave and Wireless Technology Letters, vol. 33, no. 6, pp. 831–834, 2023.
[99] E. Shepeleva, M. Makurin, G. Evtyushkin, A. Lukyanov, A. Vilenskiy, S. Chernyshev, and M. Ivashina, "Integrated w-band photoconductive switches in siw technology," IEEE Microwave and Wireless Components Letters, vol. 31, no. 7, pp. 865–868, 2021.
[100] Y. Xie, F.-C. Chen, and Q.-X. Chu, "Tunable cavity filter and diplexer using in-line dual-post resonators," IEEE Transactions on Microwave Theory and Techniques, vol. 70, no. 6, pp. 3188–3199, 2022.
[101] A. Widaa, C. Bartlett, and M. Ho¨ft, "Tunable coaxial bandpass filters based on inset resonators," IEEE Transactions on Microwave Theory and Techniques, vol. 71, no. 1, pp. 285–295, 2022.
[102] C. Che, X. Chen, L. Zhang, and M. Yu, "Multiphysics design of a resonator tuning system and dimensionless formulae," IEEE Transactions on Instrumentation and Measurement, 2023.
[103] P. Aure´lien, D. Nicolas, T. Olivier, V. Serge, and L. Carpentier, "Tunable resonator using a piston-like plunger," in 2021 IEEE MTT-S International Microwave Filter Workshop (IMFW). IEEE, 2021, pp. 233–235.
[104] K. Savin, I. Golubeva, V. Kazmirenko, Y. Prokopenko, and G. A. Vandenbosch, "Micromechanically tunable dielectric rod resonator," International Journal of Electronics and Telecommunications, pp. 615–621, 2021.
[105] C. Arnold, J. Parlebas, and T. Zwick, "Reconfigurable waveguide filter with variable bandwidth and center frequency," IEEE Transactions on Microwave Theory and Techniques, vol. 62, no. 8, pp. 1663–1670, 2014.
[106] S. Nam, B. Lee, C. Kwak, and J. Lee, "Contactless tuning plunger and its application to k-band frequency-tunable cavity filter," IEEE Transactions on Microwave Theory and Techniques, vol. 67, no. 7, pp. 2713–2719, 2019.
[107] H. Zha, I. Syratchev, D. Gudkov, and A. Grudiev, "Design of a variable x-band rf power splitter," Nuclear Instruments and Methods in Physics Research Section A: Accelerators, Spectrometers, Detectors and Associated Equipment, vol. 859, pp. 47–51, 2017.
[108] X. Liu, Y. Wei, P. Zhao, and L. Zhu, "Design of tunable bandpass filters using evanescent-mode cavity resonators," IEEE Transactions on Microwave Theory and Techniques, vol. 69, no. 7, pp. 3475–3486, 2021.
[109] F. Chen and Q. X. Chu, "Compact substrate integrated waveguide (SIW) circular cavity filters with advanced cross-coupling," IEEE Transactions on Components, Packaging and Manufacturing Technology, vol. 9, no. 1, pp. 43–51, 2019.
[110] A. Dyussembayev and D. Psychogiou, "Continuously tunable 3-d printed helical resonators and bandpass filters using actuated liquid metals," IEEE Microwave and Wireless Components Letters, vol. 32, no. 7, pp. 855–858, 2022.
[111] Y.-W. Wu, L. Qian, J. Churm, and Y. Wang, "Liquid metal-enabled filtering switches and switchplexers," IEEE Transactions on Microwave Theory and Techniques, 2024.
[112] A. Widaa, F. Kamrath, and M. Ho¨ft, "Reconfigurable TM-mode dielectric bandpass filter using liquid metals," in 2024 IEEE International Microwave Filter Workshop (IMFW). IEEE, 2024, pp. 173–175.
[113] G. Zhang, L. Xing, Q. Xu, Y. Zhao, C. Song, and Y. Huang, "A frequency tunable liquid cavity bandpass filter," Electromagnetic Science, vol. 1, no. 2, pp. 1–10, 2023.
[114] S. Alkaraki, J. Kelly, A. L. Borja, R. Mittra, and Y. Wang, "Gallium- based liquid metal substrate integrated waveguide switches," IEEE Microwave and Wireless Components Letters, vol. 31, no. 3, pp. 257–260, 2021.
[115] M. Brown and C. E. Saavedra, "Tunable branchline coupler using microfluidic channels," IEEE Microwave and Wireless Components Letters, vol. 29, no. 3, pp. 207–209, 2019.
[116] D. Jiang, Y. Liu, X. Li, G. Wang, and Z. Zheng, "Tunable microwave bandpass filters with complementary split ring resonator and liquid crystal materials," IEEE Access, vol. 7, pp. 126 265–126 272, 2019.
[117] S. Alkaraki, A. L. Borja, J. R. Kelly, R. Mittra, and Y. Gao, "Reconfigurable liquid metal-based siw phase shifter," IEEE Transactions on Microwave Theory and Techniques, vol. 70, no. 1, pp. 323–333, 2021.